Pergamon

Int. J. Heat Mass Transfer. Vol. 37, No. 15, pp. 2287–2295, 1994

0017–9310/94 $7.00+0.00

0017–9310(94)E0022–M

Transient mass transfer of a trace species in an evaporating spherical droplet with internal circulation

S. M. GHIAASIAAN

George W. Woodruff School of Mechanical Engineering, Georgia Institute of Technology, Atlanta, GA 30332-0405, U.S.A.

and

D. A. EGHBALI

Westinghouse Savannah River Company, Aiken, SC 29802, U.S.A.

(*Received* 27 *August* 1993 *and in final form* 14 *December* 1993)

Abstract—The combined heat and mass transfer during the evaporation of a superheated spherical droplet subject to an external flow field composed of its own saturated vapor, when the droplet and its surrounding vapor contain a tracer amount of a volatile transferred species, is numerically modeled. The droplet mass transfer model is an extension of the Kronig and Brink method to variable droplet radius. Gas-side heat and mass transfer are treated using the quasi-steady film theory. Calculated parameteric results, demonstrating the effects of important parameters when the partition coefficient of the transferred species is much larger than one, are presented.

1. INTRODUCTION

IN THIS paper the combined heat and mass transfer in a single droplet subject to an external gas flow field, and undergoing rapid evaporation, is modeled. The droplet Reynolds number, Re_G, is assumed to be of the order of 10–100. In this regime the droplet remains spherical and non-oscillating, and the external flow field induces an internal circulatory flow similar to the Hill's vortex flow [1]. The model is based on a direct extension of the classical Kronig and Brink's method [2], where the effect of a time-dependent droplet radius on mass diffusion inside the droplet is included. This method can also be applied to heat transfer in evaporating fuel droplets.

The combined heat and mass transfer problem represents a droplet suddenly introduced into a gaseous environment composed essentially of the droplet pure vapor, where the pressure is lower than the saturation pressure associated with the droplet temperature. Such droplets can be generated due to flashing and atomization of an initially high-pressure liquid flowing into a low-pressure environment. During the modeled evaporation process, droplet fragmentation due to internal boiling is assumed not to occur. With an assumed pure liquid, in the absence of heterogeneous nucleation sites in the droplet, internal boiling would require that the limit of superheat be reached inside the droplet. The initial droplet superheat range relevant to this study is well below the limit of superheat, however. The droplet and the surrounding gas both are assumed to contain a tracer amount of a dissolved volatile species. The transport of radionuclides by liquid droplets during a U-tube steam generator tube rupture event in a pressurized water reactor [3], and the desorption of non-condensable gases in the evaporator of an Open-Cycle Ocean Thermal Energy Conversion (OC-OTEC) system [4, 5] are two examples for the application of the stated problem. The combined heat and mass transfer during the evaporation of a droplet without an external convective flow field was addressed in [6].

Droplets subject to external flow fields have been extensively studied in the past [1, 7]. Droplets with $Re_G \approx O(100)$, in particular, have been studied for solute extraction [8–10], and more recently in spray evaporation and combustion [11–23]. Transfer of a trace species during the evaporation of a droplet, however, has not been adequately studied.

2. PREVIOUS STUDIES

Droplets with sufficiently strong surface tension, including many fluids of practical importance, remain nearly spherical up to $Re_G \approx 600$ [1]. Two major hydrodynamic regimes can be identified in the $Re_G \leqslant 500$ range. In creep flow $Re_G < 1$, the inertial effects in the momentum equations of both fluids can be neglected, and the flow remains nearly symmetrical about the equatorial plane of the sphere. For this regime analytical solutions for the flow fields in the droplet and

NOMENCLATURE

A	Hill's vortex strength [m^{-1} s^{-1}]
B_m	mass transfer driving force
C_D	drag coefficient
C_p	specific heat [J kg^{-1} K^{-1}]
C_F	frictional component of the drag coefficient
$\mathscr{D}$	mass diffusion coefficient [m^2 s^{-1}]
H^*	partition coefficient
He	Henry's number, X_s/X_u
h	coordinate scale factor
$\hat{h}_{fg}$	specific heat of vaporization [J kg^{-1}]
Ja'	modified Jakob number, $C_{PL}(T_L^0 - T_G^\infty)/\hat{h}_{fg}$
K	mass transfer coefficient [kg m^{-2} s^{-1}]
K_T	thermal conductivity enhancement factor
k	thermal conductivity [W m^{-1} K^{-1}]
M	normalized mass fraction, m/m_L^0
m	mass fraction
N	number of grid points for mass transfer
n	mass flux of the trace species [kg m^{-2} s^{-1}]
n_w	evaporation mass flux [kg m^{-2} s^{-1}]
$\mathscr{P}$	function defined in equation (8)
Pe	heat transfer Peclet number = $2Ru_{SR}/\alpha_L$
Pe_m	mass transfer Peclet number = $2Ru_{SR}/\mathscr{D}_L$
$\mathscr{Q}$	function defined in equation (9)
$\mathscr{R}$	function defined in equation (10)
R	droplet radius [m]
Re	droplet Reynolds number = $2\rho u_G^\infty R/\mu$
r	radial coordinate [m]
Sc	Schmidt number = $\nu/\mathscr{D}$
Sh	Sherwood number, defined in equations (21) and (22)
T	temperature [K]
t	time [s]
$\tilde{t}$	characteristic time [s]
U	dimensionless velocity (u/u_{SR})
u_S	liquid velocity along vortex lines [m s^{-1}]
u_{SR}	liquid velocity at droplet surface on the equator [m s^{-1}]
X	mole fraction.

Greek letters

α_L	liquid thermal diffusivity = $k_L/\rho_L C_{PL}$ [m^2 s^{-1}]
γ	droplet radius divided by droplet initial radius = R/R^0
ε	parameter defined as M_G^∞/He
ζ	variable defined as $(\eta^4 \cos^4\theta)/(2\eta^2 - 1)$
η	dimensionless radial coordinate, r/R
θ	tangential coordinate in polar spherical coordinates (Fig. 1a) [R]
κ	viscosity ratio = μ_L/μ_G
λ	variable defined as $1/2\zeta$
μ	dynamic viscosity [kg m^{-1} s^{-1}]
ξ	parameter defined as $4\eta^2(1-\eta^2)\sin^2\theta$
ρ	density [kg m^{-3}]
τ	dimensionless time, $t\alpha_L/(R^0)^2$
τ_m	dimensionless time, $t\mathscr{D}_L/(R^0)^2$
φ	azimuthal angle in polar spherical coordinate system [R]
ψ	stream function [m^3 s^{-1}]
Ω	dimensionless temperature = $(T - T_{sat})/(T_L^0 - T_{sat})$.

Subscripts

G	gas
h	hydrodynamic
L	liquid
m	mass transfer
s	s-surface (Fig. 1b)
sat	saturation
th	thermal
u	u-surface (Fig. 1b).

Superscripts

0	initial
·	high mass transfer
*	dummy variable
∞	far from the droplet.

the surrounding fluid were first obtained in [24]. At higher Re_G, the external flow field becomes increasingly asymmetric, resulting in flow separation and the formation of a wake behind the sphere. When $Re_G > 500$ the droplet will oscillate [1].

The relative motion between the droplet and the surrounding fluid induces a circulatory motion inside the droplet which strongly affects heat and mass transfer in the droplet. The Hadamard–Rybczynski solution [24] for creep flow predicts an internal circulatory motion defined by the stream function:

$$\Psi_L = \tfrac{1}{2}Ar^2(R^2 - r^2)\sin^2\theta, \tag{1}$$

where, in the absence of surface-active impurities:

$$A = \frac{u_G^\infty}{2R^2(\kappa+1)}. \tag{2}$$

The streamlines representing equation (1) are depicted schematically in Fig. 1a. At higher droplet Reynolds numbers the vortex strength will be different than equation (2): nevertheless, due to the closed streamlines, and as long as the droplet remains spheri-

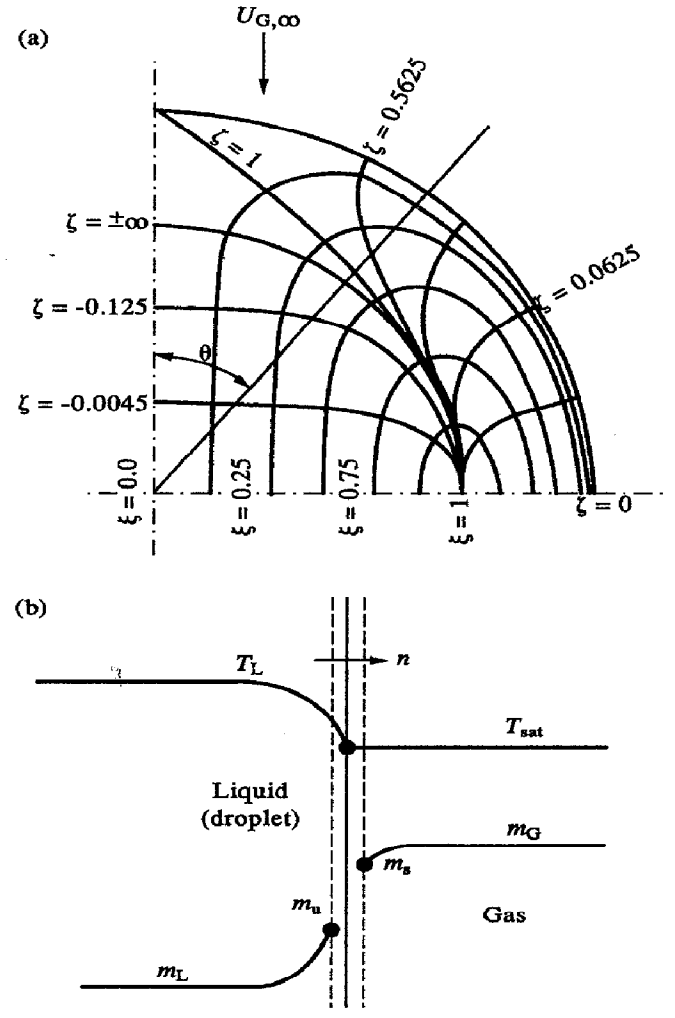

FIG. 1. Schematic of the droplet and the gas liquid interphase: (a) droplet internal circulation; and (b) the gas–liquid interphase.

cal, equation (1) approximately applies to the inviscid core of the droplet [25, 26].

Kronig and Brink [2] analyzed mass diffusion in a circulating droplet with constant radius in creep flow by using the Hadamard–Rybczynski stream functions, and casting the mass diffusion equation in the orthogonal coordinate system (ξ, ζ, φ). Since the residence time of fluid along the closed vortices is much shorter than the characteristic time for mass diffusion normal to the streamlines, the transient mass diffusion equation can be represented in a one-dimensional form, with ξ as the independent variable. Diffusion is then independent of the vortex strength [2]. The derived 1-D diffusion equation, however, is invalid very close to the droplet surface, and a concentration boundary layer forms at the droplet surface, with a thickness of the order of $R\,Pe_m^{-1/2}$ [10]. Due to the small thickness of the concentration boundary layer, however, Kronig and Brink's 1-D diffusion equation can be assumed valid up to the droplet surface [10].

Kronig and Brink's method of using the droplet internal streamlines as a coordinate and assuming uniform concentration on a closed streamline, referred to hereafter as the vortex model, has been successfully applied to heat transfer analysis of evaporating droplets [11–13, 16, 21]. The droplet core analysis in all these investigations was similar to Kronig and Brink [2], except that their orthogonal coordinate system was (ξ, λ, φ), where $\lambda = 1/(2\zeta)$ [11–13, 16, 21]. The characteristic times for the development of quasi-steady-state hydrodynamics, interior and exterior to fossil fuel droplets with $Re_G = O(100)$, are much shorter than the characteristic time for thermal diffusion in the droplet: therefore steady-state hydrodynamics can be assumed [11, 12]. The liquid-side thermal boundary layer thickness is of the order of $R\,Pe^{-1/2}$ and may not be negligible [11]. Heat and mass transfer in evaporating droplets in the $Re_G = O(10–100)$ range have also been modeled by numerically solving the 2-D (r, θ) conservation equations [15, 20, 22, 23], leading to the derivation of empirical correlations for drag and gas-side heat transfer coefficients. These numerical solutions confirm the validity of the steady-state hydrodynamic assumption in the vortex flow model [22].

The investigations dealing with the evaporation of fossil fuel droplets reviewed above address very hot gaseous environments where the gas is typically several hundred degrees K hotter than the droplet. Sensible heat transfer from the gas provides the heat for droplet evaporation. In these cases, furthermore, property changes are important due to temperature variations and the change in the concentration of various components during the droplet lifetime. Neither of these effects is significant in the problem studied here.

3. MATHEMATICAL MODEL

3.1. *General remarks*

Figure 1a depicts the droplet and the internal circulatory stream lines, and Fig. 1b is a schematic of the liquid–gas interphase. The mass fraction profiles in Fig. 1b represent conditions where transferred species mass is transferred from the gas into the liquid, and evaporation is negligible. As will be shown later, evaporation significantly modifies these profiles. The droplet is initially at $T_L^0 > T_{sat}$, and contains a dissolved volatile species with initial mass fraction $m_L^0 \ll 1$. Initial droplet superheating is assumed to be small, however: therefore the properties are assumed constant. At time $t = 0$ the droplet is introduced into an environment containing droplet vapor at $T_G^\infty = T_{sat}(P)$, where P is the ambient pressure. The vapor also contains the volatile, transferred species with mass fraction $m_G^\infty \ll 1$. The gas phase is assumed infinitely large. No chemical reactions are assumed. Using the droplet center as the reference point, the velocity of gas far away from the droplet is u_G^∞, and the droplet Reynolds number is assumed to be $O(10–100)$. The effect of interphase curvature on the equi-

librium vapor pressure (the Kelvin effect) is neglected. The flow is assumed axisymmetric.

The characteristic times associated with the development of a steady-state gas-side boundary layer, and the development of steady-state droplet internal circulation, can be estimated from

$$\tilde{t}_{G,h} = O\left(\frac{(R^0)^2}{\nu_G\, Re_G}\right)$$

and

$$\tilde{t}_{L,h} = O\left(\frac{(R^0)^2}{\nu_L\, Re_L}\right),$$

respectively [11, 21]. The characteristic heating time, and the characteristic time for mass diffusion in the droplet, furthermore, can be estimated from

$$\tilde{t}_{L,th} = O\left(\frac{(R^0)^2}{\alpha_L}\right)$$

and

$$\tilde{t}_{L,m} = O\left(\frac{(R^0)^2}{\mathscr{D}_L}\right),$$

respectively [21]. For the conditions of interest in this paper, $\tilde{t}_{L,th}$ and $\tilde{t}_{L,m}$ are both much larger than either $\tilde{t}_{L,h}$ and $\tilde{t}_{G,h}$, and quasi-steady-state hydrodynamics can be assumed.

3.2. *Mass transfer*

Mass conservation for the transferred species in the droplet can be written as:

$$\frac{\partial m_L}{\partial t} + \bar{U}_L \cdot \nabla m_L = \mathscr{D}_L \nabla^2 m_L\,. \tag{3}$$

In the (ξ, ζ, φ) coordinates, equation (3) becomes:

$$\frac{\partial m_L}{\partial t} + \frac{u_s(\xi,\zeta)}{R}\frac{1}{h_\zeta}\frac{\partial m_L}{\partial \zeta} = \frac{\mathscr{D}_L}{h_\xi h_\zeta h_\varphi}\frac{1}{R^2}\left[\frac{\partial}{\partial \xi}\left(\frac{h_\zeta h_\varphi}{h_\xi}\frac{\partial m_L}{\partial \xi}\right) + \frac{\partial}{\partial \zeta}\left(\frac{h_\xi h_\varphi}{h_\zeta}\frac{\partial m_L}{\partial \zeta}\right)\right]. \tag{4}$$

Consistent with the foregoing discussion assume $\partial m_L/\partial\zeta = 0$, and since $m_L = f(t, \xi)$:

$$\frac{\partial m_L}{\partial t} = \frac{\mathscr{D}_L}{(R^0)^2}\left(\frac{\partial m_L}{\partial \tau_{m,L}} + \frac{\partial m_L}{\partial \xi}\frac{\partial \xi}{\partial \eta}\frac{\partial \eta}{\partial \tau_{m,L}}\right). \tag{5}$$

Combining equations (4) and (5), there results:

$$\gamma^2 h_\xi h_\zeta h_\varphi \frac{\partial M_L}{\partial \tau_{m,L}} - \frac{1}{\gamma}\left(\frac{d\gamma}{d\tau_{m,L}}\right)\eta\left(\frac{\partial \xi}{\partial \eta}\right)h_\xi h_\zeta h_\varphi \frac{\partial M_L}{\partial \xi} = \frac{\partial}{\partial \xi}\left(\frac{h_\zeta h_\varphi}{h_\xi}\frac{\partial M_L}{\partial \xi}\right). \tag{6}$$

By applying $\int d\zeta$ over half of a closed streamline representing a hemisphere ($0 < \theta < \pi/2$), and noting that m_L remains unchanged along a streamline, equation (6) is recast as:

$$\gamma^2 \frac{\partial M_L}{\partial \tau_{m,L}} + 16\frac{\mathscr{R}(\xi)}{\mathscr{Q}(\xi)}\gamma\left(\frac{d\gamma}{d\tau_{m,L}}\right)\frac{\partial M_L}{\partial \xi} = \frac{16}{\mathscr{Q}(\xi)}\frac{\partial}{\partial \xi}\left(\mathscr{P}(\xi)\frac{\partial M_L}{\partial \xi}\right), \tag{7}$$

where

$$\mathscr{P}(\xi) = -\int_{\eta_1^*}^{\eta_2^*}\frac{(2\eta^2-1)^2\sin^2\theta}{\eta\cos^3\theta}\,d\zeta, \tag{8}$$

$$\mathscr{Q}(\xi) = -\int_{\eta_1^*}^{\eta_2^*}\frac{(2\eta^2-1)^2}{4\eta^3\cos^3\theta\Delta}\,d\zeta, \tag{9}$$

$$\mathscr{R}(\xi) = -\int_{\eta_1^*}^{\eta_2^*}\frac{(2\eta^2-1)^3\sin^2\theta}{8\eta\cos^3\theta\Delta}\,d\zeta, \tag{10}$$

$$\eta_1^*, \eta_2^* = [\tfrac{1}{2}(1 \mp (1-\xi)^{1/2})]^{1/2}, \tag{11}$$

$$\Delta = (1-\eta^2)^2\cos^2\theta + (2\eta^2-1)^2\sin^2\theta. \tag{12}$$

Except for the second term on the left side, which represents the effect of time dependent droplet radius, all other terms in equation (7) are identical to Kronig and Brink [2]. The initial condition for equation (7) is:

$$M_L = 1, \quad \text{for } \tau_{m,L} \leqslant 0\,. \tag{13}$$

At the center of the vortices M_L is assumed to be a regular function of ξ [10]. Therefore, at $\xi = 1$,

$$\gamma^2 \frac{\partial M_L}{\partial \tau_{m,L}} + 16\frac{\mathscr{R}(\xi)}{\mathscr{Q}(\xi)}\gamma\left(\frac{d\gamma}{d\tau_{m,L}}\right)\frac{\partial M_L}{\partial \xi} = \left(\frac{16}{\mathscr{Q}(\xi)}\frac{\partial \mathscr{P}(\xi)}{\partial \xi}\right)\frac{\partial M_L}{\partial \xi}. \tag{14}$$

Equilibrium at the interphase is represented by:

$$M_s = \frac{\rho_L}{\rho_G H^*}M_u, \tag{15}$$

where, since mass fractions are small, equation (15) can also be represented as $X_s = He\, X_u$.

Quasi-steady-state gas-phase transfer processes are assumed. These assumptions, as explained before, are reasonable. Transferred species mass conservation through the interphase gives:

$$n = n_w m_u - \rho_L \mathscr{D}_L\overline{\left(\frac{\partial m_L}{\partial r}\bigg|_{r=R}\right)} = n_w m_s + K_G'(m_s - m_G^\infty). \tag{16}$$

It can be shown that:

$$\overline{\left(\frac{\partial m_L}{\partial r}\bigg|_{r=R}\right)} = -\frac{16 m_L^0}{3R}\frac{\partial M_L}{\partial \xi}\bigg|_{\xi=0}. \tag{17}$$

Equations (15)–(17) are combined and cast in the vortex model coordinates, to get, at $\xi = 0$:

$$\frac{\partial M_L}{\partial \xi} = -\frac{3}{16}\frac{R^0\gamma}{\rho_L \mathscr{D}_L} K_G^* \times \left[\left(\frac{(1-He)n_w}{K_G^*} - He\right)M_L + M_G^\infty\right], \quad (18)$$

where [27]:

$$K_G^* = K_G \frac{\ln(1+B_m)}{B_m}, \quad (19)$$

$$B_m = \frac{M_G^\infty - M_s}{M_s - (n/n_w)}. \quad (20)$$

The following correlation is applied for calculating K_G [22]:

$$Sh_G = \frac{2K_G R}{\rho_G \mathscr{D}_G} = (1+B_m)^{-0.7}\,[2+0.87 Re_G^{1/2}\, Sc_G^{1/3}]. \quad (21)$$

It can also be shown that:

$$Sh_L = \frac{2RK_L}{\rho_L \mathscr{D}_L} = \frac{32}{3(\bar{M}_L - M_u)}\left.\frac{\partial M_L}{\partial \xi}\right|_{\xi=0}, \quad (22)$$

$$\bar{M}_L = \frac{3}{8}\int_0^1 \mathscr{Q}(\xi) M_L(\xi)\, d\xi. \quad (23)$$

3.3. *Heat transfer*

The droplet is initially superheated, and is surrounded by its own saturated vapor. Sensible heat transfer at the droplet surface is negligible [28].

For simplicity, heat transfer in the droplet is modeled using the "effective conduction" model, according to which the transient, 1-D (radial) conduction equation is applied, while the thermal conductivity is multiplied by an empirical factor to account for the effect of internal circulation. This method, originally suggested in ref. [8], has been successfully applied to non-oscillating droplets with internal circulation [21, 29, 30]. The thermal diffusion in the droplet is thus represented by:

$$\gamma^2 \frac{1}{K_T}\frac{\partial \Omega}{\partial \tau} - \gamma\eta\frac{1}{K_T}\frac{d\gamma}{d\tau}\frac{\partial \Omega}{\partial \eta} = \frac{1}{\eta^2}\frac{\partial}{\partial \eta}\left(\eta^2 \frac{\partial \Omega}{\partial \eta}\right), \quad (24)$$

where [21]:

$$K_T = 1.86 + 0.86 \tanh\,[2.245 \log_{10}(Pe/30)], \quad (25)$$

$$u_{SR} = \frac{1}{32} u_G^\infty \left(\frac{\mu_G}{\mu_L}\right) Re_G C_F, \quad (26)$$

$$C_F = 12.69 (Re_G)^{-2/3}. \quad (27)$$

The droplet Reynolds number, Re_G, is calculated assuming that the droplet is in free fall in normal gravity, where:

$$u_G^\infty = \left[\frac{8R(\rho_L - \rho_G)g}{3\rho_G C_D}\right]^{1/2}. \quad (28)$$

The drag coefficient, C_D, is calculated from [1]:

$$C_D = \frac{24}{Re_G}\left(1 + 0.15 (Re_G)^{0.687}\right). \quad (29)$$

It can be shown that, for the assumed droplet conditions, the effect of the thermal resistance associated with the droplet–gas interphase is negligible. Therefore, the initial and boundary conditions for equation (24) are: $\Omega = 1$ for $\tau \leqslant 0$; $\Omega = 0$ at $\eta = 1$; and $\partial\Omega/\partial\eta = 0$ at $\eta = 0$. Finally, energy conservation and mass continuity at the droplet surface give, at $\eta = 1$:

$$\frac{d\gamma}{d\tau} = K_T \frac{Ja'}{\gamma}\frac{\partial \Omega}{\partial \eta}, \quad (30)$$

$$n_w = -\frac{\rho_L \alpha_L}{R^0}\frac{d\gamma}{d\tau}. \quad (31)$$

4. METHOD OF SOLUTION

Equation (24) was numerically solved using the fully-implicit finite-difference technique. The spatial derivatives were central differenced, and 75 equally-spaced mesh points in the droplet radius were used. The effect of increasing the number of mesh points was tested and found to be negligibly small. Equation (30) was integrated using Euler's method. A small time-step size was used at the beginning of each calculation (typically representing $\Delta\tau = 10^{-7}$) to provide better accuracy for the fast initial transient. It was, however, increased during each numerical run, typically to 10^{-5} near the end of each calculation.

Equation (7) was also numerically solved using the fully-implicit finite-difference technique with equally-spaced mesh points in the ξ coordinate, and applying central differencing to the spatial derivatives. For consistency, the time-step $\Delta\tau$ was chosen identical to the one used in heat transfer analysis; namely, $\Delta\tau_{m,L} = \Delta\tau\, \mathscr{D}_L/\alpha_L$. The number of mesh points was 500 and was found to provide adequate numerical convergence.

Numerical values of functions $\mathscr{P}(\xi)$, $\mathscr{Q}(\xi)$, and $\mathscr{R}(\xi)$ are needed at all grid points for the numerical solution of equation (7). These were separately calculated by numerical integration of equations (8)–(10), by the trapezoidal rule, using $\Delta\zeta = 10^{-5}$ step size. Calculations were performed for $N = 200$, 300 and 500. The grids were uniform sized, therefore $\mathscr{P}(\xi)$, $\mathscr{Q}(\xi)$, and $\mathscr{R}(\xi)$ were calculated at all $\xi_i = 1 - i\,\Delta\xi$ for $i = 0, 1, 2, \ldots, N-1$, where $\Delta\xi = 1/N$. Since $\lim \mathscr{Q}(\xi) = \infty$ when $\xi \to 0$, $\mathscr{Q}(0) = 10^6$ was assumed. It is emphasized that, for each N value, tables for $\mathscr{P}(\xi)$, $\mathscr{Q}(\xi)$, and $\mathscr{R}(\xi)$ need to be calculated and stored only once. Calculated

Table 1. Numerical values of the function $\mathscr{R}(\xi)$

ξ	$\mathscr{R}$
1.0	0.0
0.9	4.2027×10^{-2}
0.8	8.4894×10^{-2}
0.7	1.2879×10^{-1}
0.6	1.7390×10^{-1}
0.5	2.203×10^{-1}
0.4	2.6835×10^{-1}
0.3	3.1851×10^{-1}
0.2	3.7155×10^{-1}
0.1	4.2923×10^{-1}

values of $\mathscr{R}(\xi)$ are summarized in Table 1. Values of $\mathscr{P}(\xi)$ and $\mathscr{Q}(\xi)$ can be found in ref. [2].

5. RESULTS AND DISCUSSION

To establish the correctness of the solution method, mass transfer calculation results of Brignell [10] were reproduced by applying $\hat{h}_{fg} \to \infty$ (constant droplet radius) and M_L = constant at $\eta = 1$ (constant concentration at droplet surface), with good agreement. These solutions, in the limit of $\tau \to \infty$, gave $Sh_L \to 17.9$, in agreement with ref. [2]. Parametric results relevant to the transfer of radioiodine during the evaporation of relatively large droplets during a U-tube steam generator tube rupture (SGTR) event in a pressurized water reactor are presented below. However, directly-applicable experimental or analytical results are not available for comparison.

The properties chosen for the results to be presented are for a superheated water droplet, with $R^0 = 100$ μm, undergoing evaporation in an ambient pressure of 70 atm. Therefore $\rho_L = 740$ kg m^{-3}, $\rho_G = 36.5$ kg m^{-3}, $\hat{h}_{fg} = 1.505 \times 10^6$ J kg^{-1}, and $\alpha_L = 1.43 \times 10^{-7}$ m^2 s^{-1}. The properties of the transferred species were varied parametrically, representing the estimated transport properties of iodine in water and steam. The release of radioiodine is an important concern in certain nuclear reactor incidents, in particular during a U-tube steam generator tube rupture (SGTR) incident in pressurized water reactors. At 70 atm which represents the typical operating pressure in the secondary side of a steam generator, for iodine, $\mathscr{D}_L \approx 2.40 \times 10^{-8}$ m^2 s^{-1} and $\mathscr{D}_G \approx 5.0 \times 10^{-7}$ m^2 s^{-1} are estimated [3]. The magnitude of H^*, however, is not accurately known, and may depend on the water pH and iodine concentration [31]. The prototypical value has been estimated to be of the order of 10^2–10^4 for parametric and sensitivity calculations [3]. The assumed properties were thus varied in the range $10^{-9} \leqslant \mathscr{D}_L \leqslant 10^{-4}$ m^2 s^{-1}; $10^{-9} \leqslant \mathscr{D}_G \leqslant 10^{-5}$ m^{-2} s^{-1}, and $50 \leqslant H^* \leqslant 5 \times 10^3$. The primary coolant in a pressurized water reactor is subcooled water at typically 150 atmosphere pressure. The initial droplet superheat associated with this example is therefore $\approx$ 10–30 K. Thus, the droplet initial superheat was

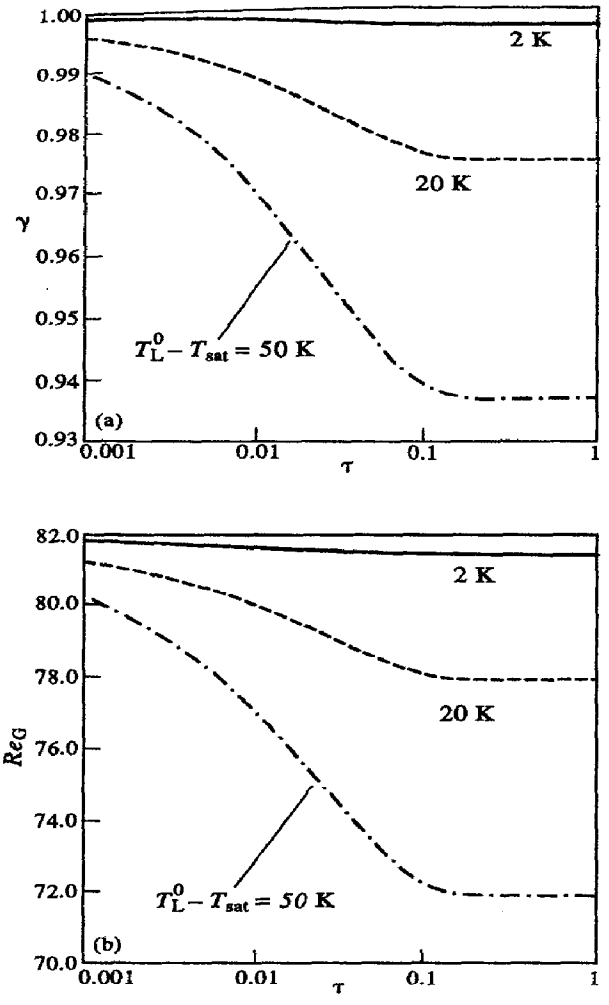

FIG. 2. Variation of droplet size and Reynolds number with time: (a) dimensionless droplet radius; and (b) droplet Reynolds number.

varied in the range $0.02 \leqslant \theta_0 \leqslant 50$ K in order to examine the trends and limits of the results.

Figure 2a and b depicts the variations, with time, of the droplet dimensionless radius and Reynolds number, respectively, with the initial droplet superheat temperature as the parameter. As noted, evaporation is essentially completed at $\tau \approx 0.1$, and Re_G remains in the 10–100 range. The predicted dimensionless temperature histories indicated very small effects of the droplet initial superheat.

The predicted variations of the droplet mean mass fraction, $\bar{M}_L$, with time are shown in Fig. 3, where the droplet initial superheat is maintained constant, and M_G^∞ and H^* are both varied parametrically. $\bar{M}_L$ remains approximately unchanged early in the transient when significant evaporation is underway, where $\bar{M}_L$ is insensitive to the magnitudes of M_G^∞ or H^* due to the slow mass diffusion in the droplet. Following the completion of evaporation at $\tau \approx 0.1$, the parameter determining the direction of mass transfer is:

$$\frac{\rho_G H^* M_G^\infty}{\rho_L \bar{M}_L},$$

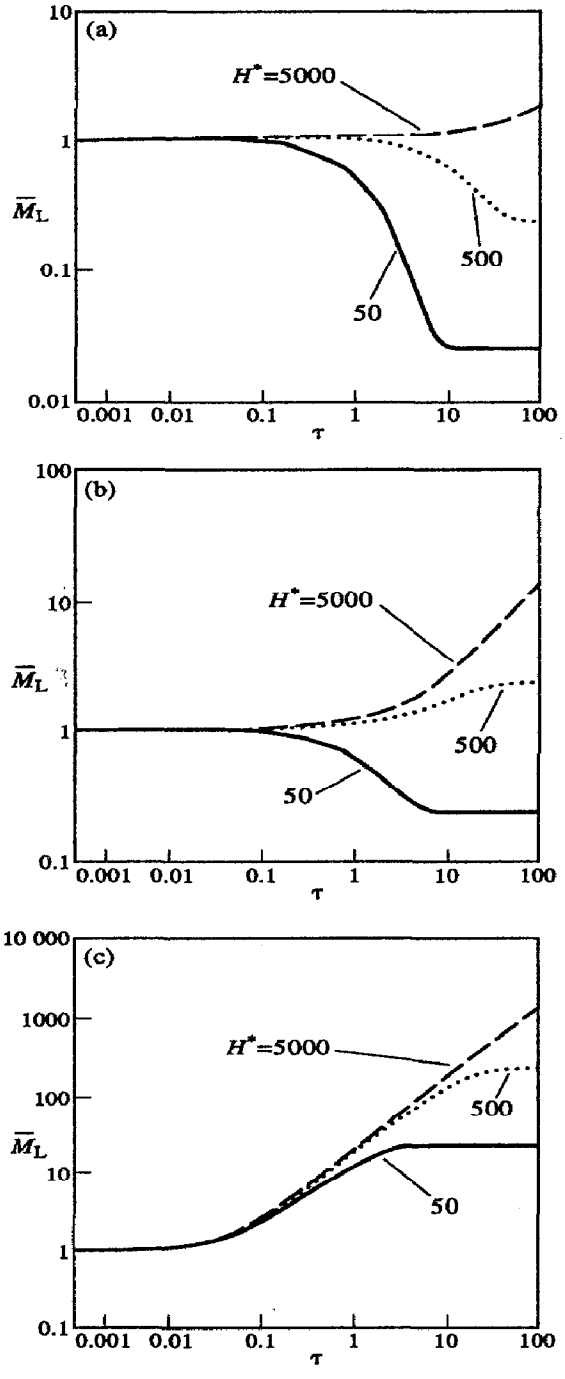

FIG. 3. The effects of partition coefficient and the gas ambient mass fraction on the mean droplet mass fraction ($T_L^0 - T_{sat} = 20$ K): (a) $M_G^\infty = 0.01$; (b) $M_G^\infty = 0.1$; and (c) $M_G^\infty = 10$.

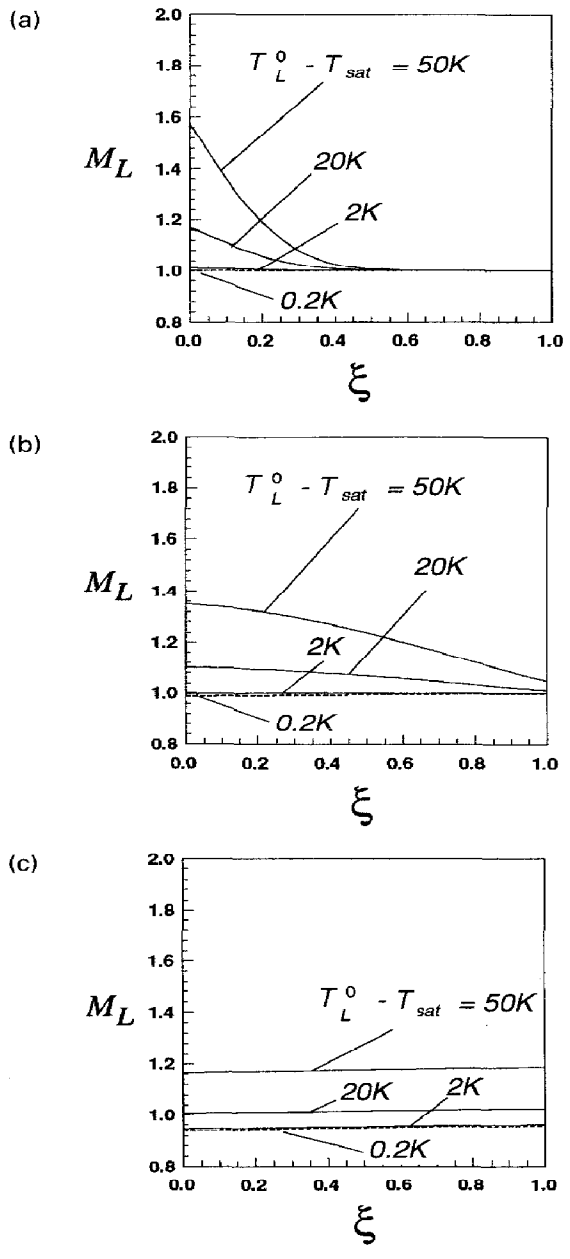

FIG. 4. The effects of initial droplet superheat and gas ambient mass fraction on droplet mass fraction profiles ($H^* = 500$, $M_G^\infty = 0.01$): (a) $\tau = 0.01$; (b) $\tau = 0.1$; and (c) $\tau = 1.0$

which is approximately equal to ε here since $\bar{M}_L \approx 1$. With $\varepsilon > 1$ mass transfer takes place from the gas into the droplet, and vice versa. As a result, for $M_G^\infty = 0.01$, for example, with $H^* = 50$ and 500, desorption takes place from the droplet, and for $H^* = 5000$ mass transfer takes place from the gas into the droplet. The duration of the transient mass transfer period leading to an equilibrium between the droplet and the surrounding vapor, represented in the figures by a horizontal line, monotonically increases with increasing H^*.

Typical mass fraction profiles in the droplet are shown in Fig. 4, where $\xi = 1$ and 0 represent the center of the vortices and the droplet surface, respectively (see Fig. 1a). Mass fraction distributions on the vortices are depicted at three time snapshots for a transient where $\varepsilon = 0.25$, indicating that in the absence of evaporation mass desorption should take place from the droplet. Due to the evaporation, however, mass fraction in the droplet outer layers initially increases. This increase is because the mass fraction of the transferred species in the evaporated mass, which is determined by equilibrium at the interphase, see equation

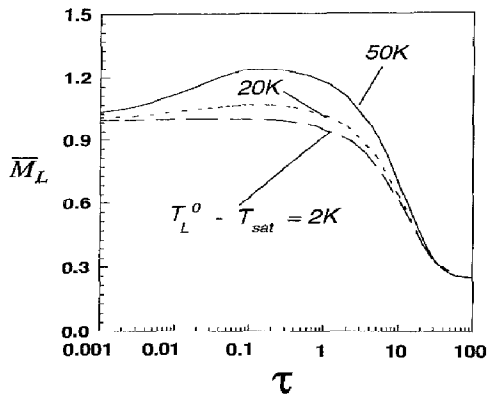

FIG. 5. The effect of initial droplet superheat on the mean droplet mass fraction ($H^* = 500$, $M_G^\infty = 0.01$).

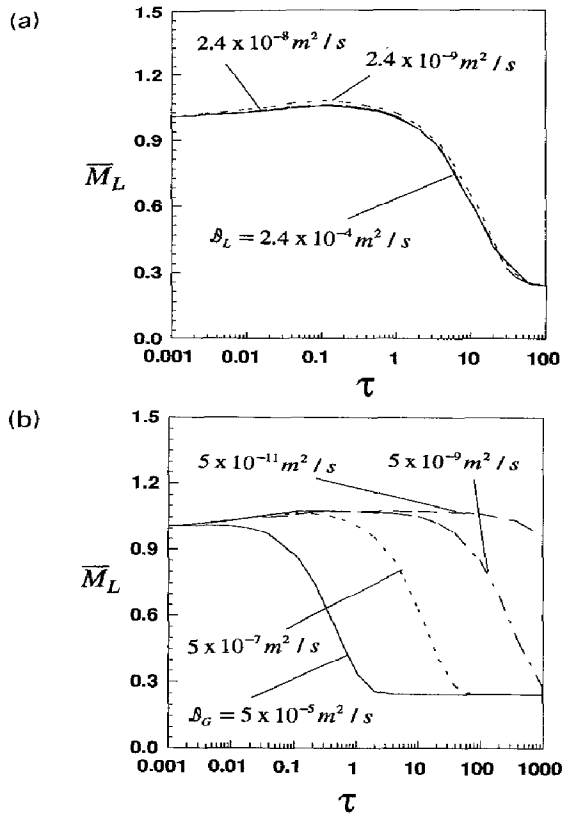

FIG. 6. The effects of the mass diffusion coefficients on the mean droplet mass fraction: (a) the effect of liquid-side mass diffusion coefficient ($H^* = 500$, $M_G^\infty = 0.01$, $T_L^0 - T_{sat} = 20$ K, $\mathscr{D}_G = 5 \times 10^{-7}$ m^2 s^{-1}); and (b) the effect of gas-side mass diffusion coefficient ($H^* = 500$, $M_G^\infty = 0.01$, $T_L^0 - T_{sat} = 20$ K, $\mathscr{D}_L = 2.4 \times 10^{-8}$ m^2 s^{-1}).

(15), is lower than initial droplet mass fraction. A higher initial droplet superheat results in a higher evaporation mass flux, leading to a more significant initial increase in the mass fraction in the droplet. The desorbed gas, which in the case of a stagnant droplet would accumulate in a layer blanketing the droplet and strongly affecting its mass transfer behavior [6], is blown away consistent with the quasi-steady boundary layer modeling of the gas-side mass transfer process. Following the termination of the evaporation the diffusion process in the droplet approaches a quasi-steady-state represented by a relatively flat mass fraction profile (Fig. 4c). The temporal variations of $\bar{M}_L$ for these droplets are shown in Fig. 5 and confirm that the effect of the droplet initial superheat on the droplet mass transfer process is strong for a significantly long time after evaporation has terminated at around $\tau \approx 0.1$, and disappears only when the droplet approaches equilibrium with the surrounding vapor.

Figure 6a shows the effect of liquid-side mass diffusivity on the temporal variations of $\bar{M}_L$. Note that $\mathscr{D}_L = 2.4 \times 10^{-8}$ m^2 s^{-1} represents the physical problem modeled here. Due to the small gas-side mass diffusivity, increasing $\mathscr{D}_L$ by four orders of magnitude does not noticeably affect the overall transient mass transfer, indicating the gas-side controlled nature of the process. Decreasing $\mathscr{D}_L$ by an order of magnitude, however, renders the liquid- and gas-side mass transfer resistances comparable and significantly reduces the mass transfer rate. The gas-side controlled nature of the process is further confirmed by Fig. 6b, which indicates that the droplet mass transfer is quite sensitive to the gas-side mass diffusivity.

6. CONCLUDING REMARKS

The combined heat and mass transfer in an evaporating droplet with internal circulation was modeled by extending the method of Kronig and Brink to variable droplet radius. The gas-side heat and mass transfer were treated using the quasi-steady film model. Parametric calculations relevant to the transport of iodine during a U-tube steam generator tube rupture event in a pressurized water reactor were presented.

REFERENCES

1. R. Clift, J. R. Grace and M. E. Weber. *Bubbles, Drops, and Particles*. Academic Press, New York (1978).
2. R. Kronig and J. C. Brink, On the theory of extraction from falling droplets, *Appl. Scient. Res.* **A2**, 142–154 (1951).
3. S. M. Ghiaasiaan and A. T. Wassel, STARRS-MMS Code: evaluating steam generator tube ruptures. Electric Power Research Institute Report, EPRI NP-6668-CCML, Palo Alto, CA (1990).
4. D. Bharathan and F. Kreith, Heat transfer research for ocean thermal energy conversion, *J. Heat Transfer* **110**, 5–22 (1988).
5. S. M. Ghiaasiaan, A. T. Wassel and C. S. Lin, Direct contact condensation in the presence of non-condensables for OC-OTEC, *J. Solar Energy Eng.* **113**, 228–235 (1991).
6. S. M. Ghiaasiaan and D. Luo, Transient mass transfer at the surface of an evaporating stationary droplet, *Int. J. Heat Mass Transfer* **37**, 461–468 (1994).
7. V. E. Levich. *Physico Chemical Hydrodynamics*. Prentice-Hall, Englewood Cliffs, NJ (1962).
8. P. H. Calderbank and I. J. O. Korchinski, Circulation in liquid drops, *Chem. Eng. Sci.* **6**, 65–78 (1956).
9. L. E. Johns and R. E. Beckman, Mechanisms of dispersed-phase mass transfer in viscous, single-drop extraction system, *A.I.Ch.E. J.* **12**, 10–16 (1966).
10. A. S. Brignell, Solute extraction from an internally cir-

culating spherical liquid droplet, *Int. J. Heat Mass Transfer* **18,** 61–68 (1975).
11. S. Prakash and W. A. Sirignano, Liquid fuel droplet heating with internal circulation, *Int. J. Heat Mass Transfer* **21,** 885–895 (1978).
12. S. Prakash and W. A. Sirignano, Theory of convective droplet vaporization with unsteady heat transfer in circulating liquid phase, *Int. J. Heat Mass Transfer* **23,** 253–268 (1980).
13. A. Y. Tong and W. A. Sirignano, Analytical solution for diffusion and circulation in a vaporizing droplet, *Ninth Symposium (International) on Combustion*, The Combustion Institute, Pittsburgh, pp. 1007–1020 (1982).
14. M. Renksizbulut and M. C. Yuen, Experimental study of droplet evaporation in a high-temperature air stream, *J. Heat Transfer* **105**, 384–388 (1983).
15. M. Renksizbulut and M. C. Yuen, Numerical study of droplet evaporation in a high-temperature stream, *J. Heat Transfer* **105,** 389–397 (1983).
16. S. K. Aggarwal, A. Y. Tong and W. A. Sirignano, A comparison of vaporization models in spray calculations, *AIAA J.* **22,** 1448–1457 (1984).
17. A. Y. Tong and W. A. Sirignano, Multicomponent transient droplet vaporization with internal circulation: integral equation formulation and approximate solution, *Numer. Heat Transfer* **10,** 253–278 (1986).
18. A. Y. Tong and W. A. Sirignano, Multicomponent droplet vaporization in a high temperature gas, *Combustion and Flame* **66,** 221–235 (1986).
19. S. K. Aggarwal, Modeling of a dilute vaporizing multicomponent fuel spray, *Int. J. Heat Mass Transfer* **30,** 1949–1961 (1987).
20. M. Renksizbulut and R. J. Haywood, Transient droplet evaporation with variable properties and internal circulation at intermediate Reynolds numbers, *Int. J. Multiphase Flow* **14,** 189–202 (1988).
21. B. Abramzon and W. A. Sirignano, Droplet vaporization model for spray combustion calculations, *Int. J. Heat Mass Transfer* **32,** 1605–1618 (1989).
22. R. J. Haywood, R. Nafziger and M. Renksizbulut, A detailed examination of gas and liquid phase transient processes in convective droplet evaporation, *J. Heat Transfer* **111,** 495–502 (1989).
23. M. Renksizbulut and M. Bussmann, Multicomponent droplet evaporation at intermediate Reynolds numbers, *Int. J. Heat Mass Transfer* **36,** 2827–2835 (1993).
24. J. Hadamard, Mouvement permanente lent d'une sphere liquide et visqueuse dans un liquid visqueux. *C. R. Hebd. Seanc. Acad. Sci. Paris* **152,** 1735–1817 (1911).
25. G. K. Batchelor, On steady laminar flow with closed streamlines at large Reynolds number, *J. Fluid Mech.* **1,** 177–190 (1956).
26. J. F. Harper and D. W. Moore, The motion of a spherical liquid drop at high Reynolds number, *J. Fluid Mech.* **32,** 367–391 (1968).
27. D. K. Edwards, V. E. Denny and A. F. Mills, *Transfer Processes* (2nd Edn). Hemisphere Publishing, Washington (1979).
28. A. F. Mills, Condensation heat transfer: comments on non-equilibrium temperature profiles and the engineering calculation of mass transfer, *Int. J. Multiphase Flow* **6,** 41–50 (1980).
29. J. D. Jin and G. L. Borman, A model for multi-component droplet vaporization at high ambient pressures, *Combustion Emission Analysis P-***126,** 213–223, SAE Inc. (1985).
30. D. G. Talley and S. C. Yao, A semi-empirical approach to thermal and composition transients inside vaporizing fuel droplets, *Twenty-first Symposium (International) on Combustion*, The Combustion Institute, pp. 609–616 (1986).
31. E. C. Beahm, S. R. Daish, J. Hopenfeld, W. E. Shockley and P. Voilleque, Iodine speciation and partitioning in PWR steam generator tube rupture. U.S. Nuclear Regulatory Commission Report NUREG-1108 (1985).